Metallophysics and Advanced Technologies
Металофіз. новітні технол.
Metallofiz. Noveishie Tekhnol.
2026, vol. 48, No. 3, pp. 259–273
https://doi.org/10.15407/mfint.48.03.0259
Reprints available directly from the publisher

PACS numbers: 61.72.Ff, 61.72.Qq, 62.20.M-, 81.16.Rf, 81.20.Vj, 81.40.Lm, 81.70.Bt

The Influence of the Distribution of Alloying Elements on the Structure and Properties of Aircraft Engine Parts in Additive Manufacturing

M. Gnatenko*, H. Laptieva*, V. Yefanov*, O. Kalinichenko*, R. Osipchuk**

**Zaporizhzhia Polytechnic National University,*
64 Zhukovsky Str.,
UA-69063 Zaporizhzhia, Ukraine
***Ukrainian State University of Science and Technology,*
2 Lazaryan Str.,
UA-49000 Dnipro, Ukraine

This paper presents the method and results of producing the aeroengine components from EP648 superalloy *via* plasma surfacing. Material-characterisation work is conducted on the additively grown samples by means of the microstructure examination and mechanical testing. The samples obtained by plasma surfacing demonstrate superior mechanical properties compared to the traditionally cast material and reach the levels of wrought material with the exception of room-temperature elongation. The same process is used to produce an aeroengine-turbine casing, which is found free of unacceptable metallurgical defects and in full compliance with the quality specifications. The combined assessment results have validated plasma surfacing an acceptable method of manufacture for structural and stator aeroengine parts using EP648 superalloy.

Key words: wire arc additive manufacturing, plasma surfacing, superalloy, turbine.

Corresponding author: Mikhaylo Gnatenko
E-mail: gnatenkomike66@gmail.com

Citation: M. Gnatenko, H. Laptieva, V. Yefanov, O. Kalinichenko, and R. Osipchuk, The Influence of the Distribution of Alloying Elements on the Structure and Properties of Aircraft Engine Parts in Additive Manufacturing, *Metallofiz. Noveishie Tekhnol.*, **48**, No. 3: 259–273 (2026). DOI: 10.15407/mfint.48.03.0259

У статті представлено методику та результати виготовлення компонентів авіяційних рушіїв з жароміцного стопу ЕП648 методою плазмового натоплення. Дослідження властивостей матеріялу зразків, одержаних адитивним методом, проводили шляхом аналізи мікроструктури та механічних випробувань. Зразки, одержані методою плазмового натоплення, показали поліпшені механічні властивості порівняно з традиційно литим матеріялом і досягли рівня деформованого матеріялу (за винятком видовження за кімнатної температури). Той самий процес був застосований для виготовлення корпусу турбіни авіяційного рушія, який не виявив неприпустимих металурґійних дефектів і повністю відповідав вимогам якости. Сукупні результати оцінки підтвердили прийнятність плазмового натоплення як методу виготовлення конструкційних і статорних деталів авіяційних рушіїв із застосуванням стопу ЕП648.

Ключові слова: адитивне виробництво з використанням дугового дроту, плазмове натоплення, жароміцний стоп, турбіна.

(Received 2 April, 2025; in final version, 16 July, 2025)

1. INTRODUCTION

Wire Arc Additive Manufacturing (WAAM) is an additive manufacturing method that grows a part blank layer-by-layer by melting a filler wire using a heat source. Compared with other additive manufacturing processes, WAAM has its advantages over powder-based additive methods due to a much higher material utilization factor, higher growth speed and closer to net-shape of the produced blanks [1, 2]. These cost-effective advantages have made WAAM particularly attractive to aeroengine manufacturers in the production of medium to large stator and structural components.

WAAM, also known as in-mould welding, in-mould fusion, and 3*D*-welding [6, 7], is based on the concepts of automated welding processes such as metal gas arc welding [3], microplasma welding [4] and inert gas welding with tungsten electrodes [5]. The material build-up speed of this process can reach up to 160 g/min, depending on the type of material and process parameters [8], making it capable of producing medium to large-size parts in short periods of time [9–11]. Among the heat sources, plasma arc has an energy density lower than laser (in exchange for higher intensity), but higher than other electric arc sources [13]. The combined benefit of relatively low cost, high dimensional accuracy and low probability to result in metallurgical defects in the products [12] has made plasma surfacing an attractive process, compared to other forms of WAAM, in producing high-value adding components.

The main process parameter of a plasma torch is its current, ranging from 15 A to 250 A [15], to produce a concentrated and stable arc. A

good level of control for the welding pool geometry can be achieved by maintaining the stability of the plasma arc and the smoothness of the wire feed [14].

The plasma-surfacing process has a relatively low additive growth rate, lower than 1.0 g/min [16], compared with other processes. However, the low heat input of the plasma arc ensures high surface cleanliness [17], which is beneficial for the production of more quality-demanding aeroengine components. It has been found possible to use plasma surfacing to obtain additively grown products with mechanical properties not only comparable to castings, but also in some cases at the levels of forgings.

The aeroengine stator and structural parts are particularly cost sensitive. These parts are often made from superalloys using conventional casting, forging or stamping processes, involving expensive design and manufacture work for the moulds and dies. The blanks are subsequently subject to complicated and time-consuming machining processes to remove excessive stock margins. The combined impact of high processing cost and low material utilization factor makes such parts ideal candidates for implementing the plasma-surfacing process as an alternative and more cost-effective manufacturing method. Therefore, the work presented in this paper was carried out to experiment and validate the plasma-surfacing process in the manufacture of superalloy aeroengine parts in an attempt to achieve mechanical properties close to the levels of forgings.

2. MATERIALS AND EXPERIMENTAL METHODS

EP648 is a nickel-based superalloy developed originally in the former Soviet Union in the late 1970s. Over the years, EP648 has been widely adopted as a wrought alloy mainly for the stator and structural components of aeroengines. The cast variant of EP648 bears the grade designation VKh4L, often produced from revert or rejected EP648 material. Eastern European aeroengine manufacturer has extensive use of both EP648 and VKh4L alloys across all of its engine families.

The plasma-surfacing process in this work was carried out in a fully automated robotic cell consisting of an SBI TP200-R plasma torch, a PMI-350 AC/DC TL plasma power supply and a FANUC M-710iC 6-axis industrial robot. A rigidly fixed steel substrate was used as the base to build the samples upon, as shown in Fig. 1. A 5mm-long plasma arc was generated on the plasma torch by applying a current of 85–-100 A at 20 V on the power supply. The plasma arc was concentrated on an EP648 superalloy wire of 1.0 mm in diameter, which was continuously fed at a rate of 0.8 mm/min by an automatic wire dispenser. The plasma torch and wire dispenser were attached to the robotic arm and traversing at constant speed of 4.0 mm/s over the substrate. The gas

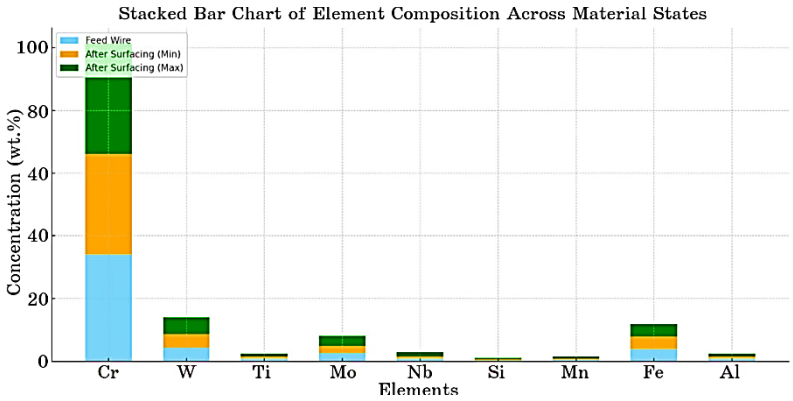

Fig. 1. Comparative analysis of elemental composition in EP648 alloy across different states: initial feed wire and permissible ranges after plasma surfacing (min–max values, wt.%).

consumption rate during the plasma-surfacing process was set at 12 L/min. With this setup, EP648 superalloy sample plates measuring 200×150×20 mm were grown on the substrate.

The chemical composition of the samples was investigated by x-ray fluorescence (XRF) spectroscopy using an Olympus DPO-2000 portable spectrometer. The SPECTROMAX optical emission spectrometer has also been used to more accurately measure certain elements such as titanium carbides and carbonitrides. The microstructure of the samples was studied by means of optical and electronic metallography.

The additively grown sample plates were subject to the standard heat treatment for EP648 superalloy including solutioning at 1140°C for 1 hour, followed by ageing at 900°C for 16 hours. Specimen blocks were then diced out of the sample plates and machined into cylindrical test bars according to the scheme shown in Fig. 1 both in the longitudinal and transverse directions relative to the growing axis of the samples.

Mechanical testing was then conducted on the test bars according to ISO 6892 standard using a universal tensile machine. The properties of interest are ultimate tensile strength ($\sigma_{в}$,), yield strength $\sigma_{0.2}$, and elongation at break (δ). The obtained results were processed by applying statistical methods used for experimental data and by secant method. To investigate the microstructures of the samples, a combined method was applied, which included qualitative and quantitative studies using optical and electronic metallography as well as micro-x-ray spectral analysis. The chemical composition, microstructure and mechanical properties of the studied samples were all determined using production-proven methods and equipment, with measurement errors less than 5% due to measurement uncertainty.

TABLE 1. Chemical composition of surfaced alloy.

Material type	Composition by weight, %									
	Ni	Cr	W	Ti	Mo	Nb	Si	Mn	Fe	Al
Feed wire	Matrix	34,2	4,41	0,95	2,66	0,97	0,4	0,5	4,0	0,99
Alloy after plasma surfacing	Matrix	33,0–36,0	4,2–5,2	0,6–1,0	2,2–3,1	0,5–1,2	0,4	0,45	4,0	0,6–10
Nominal composition of EP648	Matrix	32,0–35,0	4,3–5,3	0,5–1,1	2,3–3,3	0,5–1,5	0,4	0,5	4,0	0,5–1,1

Table 1 presents a detailed chemical composition analysis of EP648 alloy at different manufacturing stages. A comparative analysis reveals three key material states: initial feed wire, post-plasma-surfacing condition, and nominal alloy composition.

The matrix element (nickel) serves as the base, while alloying elements form a complex strengthening system. Chromium, ranging from 32.0–35.0 wt.%, provides protective oxide film formation and enhances corrosion resistance. Refractory elements, tungsten (4.3–5.3 wt.%) and molybdenum (2.3–3.3 wt.%), contribute to solid-solution strengthening and improved heat resistance. Of particular interest is the microalloying system, including titanium (0.5–1.1 wt.%) and niobium (0.5–1.5 wt.%), which participate in the formation of strengthening intermetallic phases. The presence of silicon (0.4 wt.%), manganese (0.5 wt.%), iron (4.0 wt.%), and aluminium (0.5–1.1 wt.%) is attributed to technological aspects of production and their influence on physical and mechanical properties. Comparative analysis demonstrates that the plasma-surfacing process maintains chemical composition within nominal values, indicating process stability and high material quality. The diagram shows the comparative distribution of chemical elements in EP648 alloy across different states. Light blue bars represent the elemental content in the initial feed wire, while orange and green colours indicate minimum and maximum values after plasma surfacing, respectively. Chromium (Cr) is the primary alloying element at approximately 34%. Significant concentrations are also observed for tungsten (W) at ≅4–5% and iron (Fe) at ≅4%. Other elements (Ti, Mo, Nb, Si, Mn, Al) are present in lower quantities, not exceeding 3%.

Notably, the post-surfacing composition ranges (min–max) encompass the feed wire values, indicating process stability and preservation of chemical composition.

3. RESULTS AND DISCUSSIONS

The measurement results for the chemical composition of the grown samples are presented in Table 1, in comparison to the nominal composition of the EP648 superalloy and the measured values of the feeding wire. It is clear that the chemical composition of the samples grown by the plasma-surfacing method corresponds to that of the feeding wire, which in turn meets the EP648 alloy specification.

Microstructural analysis was carried out on the cross sections of the samples cut in both longitudinal and transverse directions relative to the growth axis, as shown in Fig. 2. It can be seen that the microstructure of the samples consists of a γ-solid solution with a large number of nitrides and carbonitrides. The microstructure of the plasma-surfaced samples resembles that of typical cast samples, only with an increased number of nitrides and carbonitrides, as well as larger carbide clusters along the grain boundaries.

The fusion lines are not visible in the microstructure (Fig. 3). The microstructure exhibits a good degree of homogeneity characterized by the epitaxial growth of grains across the deposited layers.

The reason why the microstructure of the grown samples does not

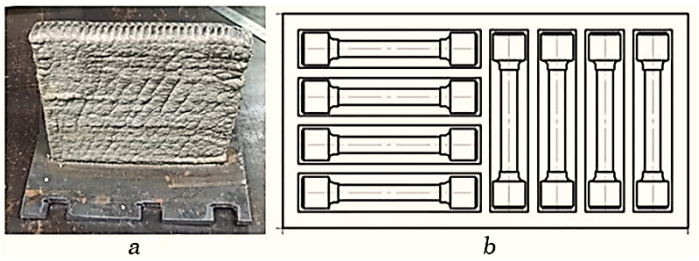

Fig. 2. Samples manufactured using plasma surfacing: (*a*) sample plate on substrate; (*b*) test bar cutting scheme.

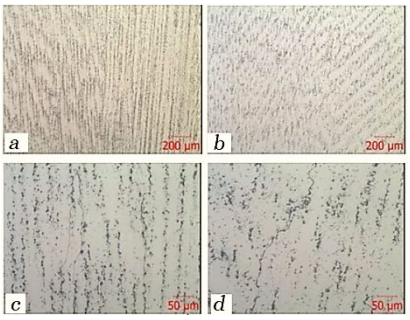

Fig. 3. Microstructure of EP648 samples after plasma surfacing: (*a*) ×100, transverse direction; (*b*) ×100, longitudinal direction; (*c*) ×200, transverse direction; (*d*) ×200, longitudinal direction.

differ significantly from the cast structure is that the formation of the microstructure in the plasma-surfacing process follows a similar mechanism as in the cast process. However, the microstructure obtained by the plasma-surfacing method is characterized by a smaller grain size compared to the cast microstructure. This is due to the fact that the volume of the molten metal is smaller in plasma surfacing than in the casting process, which leads to a higher cooling and crystallization rate. Due to the increased number of grains and the compactness of the crystalline structure, it is more conducive for nanostructures such as nitro carbides and titanium carbides to form in the alloy matrix. As a result, the additively grown material after plasma surfacing has a more compact grain structure, which in theory offers better heat resistance.

3.1. X-Ray Spectral Microanalysis of EP648 (VKh4L) Alloy Chemical Composition

X-ray spectral microanalysis (XSMA) of the samples, performed at

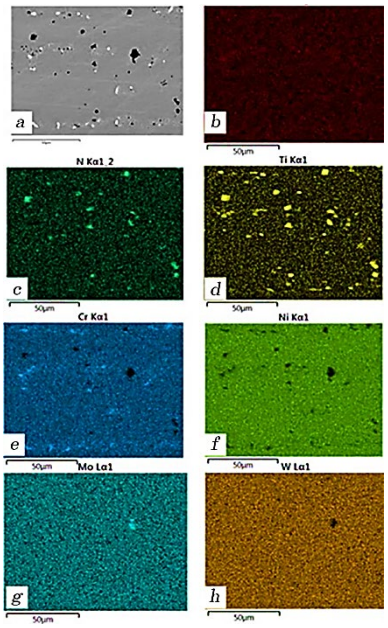

Fig. 4. X-ray spectral microanalysis of EP648 (VKh4L) alloy chemical composition. (*a*) microstructure of the sample; (*b*) carbon (C) distribution map; (*c*) nitrogen (N) distribution map; (*d*) titanium (Ti) distribution map; (*e*) chromium (Cr) distribution map; (*f*) nickel (Ni) distribution map; (*g*) molybdenum (Mo) distribution map, (*h*) tungsten (W) distribution map.

×1000 magnification (Fig. 4), reveals characteristic features of chemical elements distribution in the investigated material. The element distribution maps clearly show the microstructure of heat-treated samples.

Distribution maps of the main alloying elements (Ni, Cr, W, Ti) demonstrate their uniform distribution throughout the studied area. The colour intensity in the maps is directly proportional to the element concentration at a given point, allowing visual assessment of local composition variations.

Of particular interest is the distribution of titanium, which forms the strengthening TiN phase. The corresponding distribution map shows uniformly distributed inclusions of increased concentration, indicating the formation of dispersed titanium nitride particles.

Analysis of chromium and tungsten distribution indicates the presence of carbide phases characteristic for this alloy class. These elements demonstrate co-ordinated distribution, which is typical for complex carbides.

The nickel-based γ-matrix phase is characterized by homogeneous distribution of alloying elements, indicating the absence of significant chemical heterogeneity and segregation phenomena in the material.

Quantitative analysis confirms the compliance of chemical composition with the requirements of Technical Specification 1-809-45-2011 for EP648 (VKh4L) alloy. The observed element distribution and morphology of structural constituents indicate properly conducted heat treatment of the material (Fig. 5).

The presented graph demonstrates the distribution characteristics

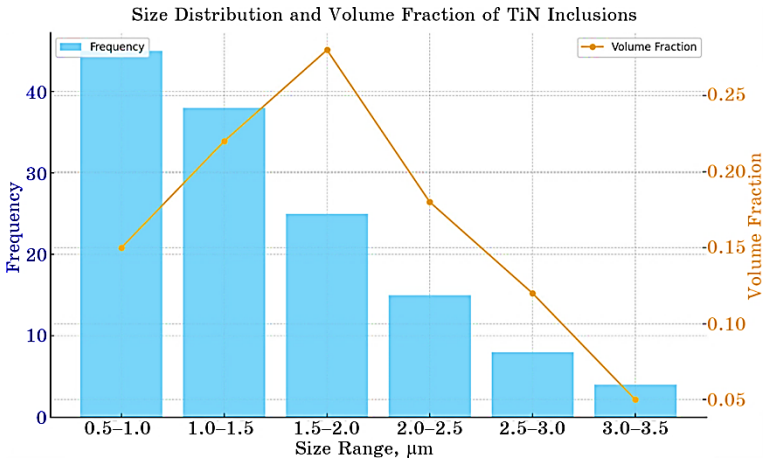

Fig. 5. Size distribution and volume fraction of TiN inclusions in EP648 alloy microstructure; histogram shows frequency distribution (blue bars), line represents volume fraction (orange line).

of TiN inclusions in the EP648 alloy microstructure. The analysis reveals a significant concentration of fine particles, with the highest frequency observed in the 0.5–1.0 μm size range, reaching 45 occurrences. Notably, while smaller particles dominate numerically, the volume fraction shows a distinct maximum of 0.28 for inclusions in the 1.5–2.0 μm range. This bimodal distribution pattern suggests optimal precipitation conditions during the heat treatment process. The frequency and volume fraction both exhibit a consistent declining trend for particles larger than 2.0 μm, with minimal presence in the 3.0–3.5 μm range. The predominance of fine TiN inclusions, particularly in the sub-micron and near-micron ranges, indicates favourable conditions for maintaining the alloy mechanical properties through effective dispersion strengthening mechanisms. This size distribution pattern aligns with typical requirements for high-performance nickel-based superalloys, where fine, uniformly distributed particles contribute to enhanced structural stability and mechanical performance.

The tensile test results at room temperature are shown in Fig. 6, where the ultimate strength ($\sigma_в$,), yield strength ($\sigma_{0.2}$), and elongation at break (δ) of the additively grown samples are compared with the conventionally wrought and cast specifications. Seven longitudinal and five transverse samples were tested and the error bars in Fig. 3 show the maximum and minimum values acquired in the tests. It is clear that the ultimate strength ($\sigma_в$) of the additively grown samples at room temperature satisfy the wrought and cast. The yield strength ($\sigma_{0.2}$) far exceeds the requirement of wrought EP648 by a large margin. It is worth noting that although no specification limit of yield strength exists for the cast VKh4L material; it is highly unlikely that the cast VKh4L material would exhibit any better yield strength values than its wrought counterpart would. The elongation at break (δ) result at room temperature exceeds the specification of cast material, but is below the

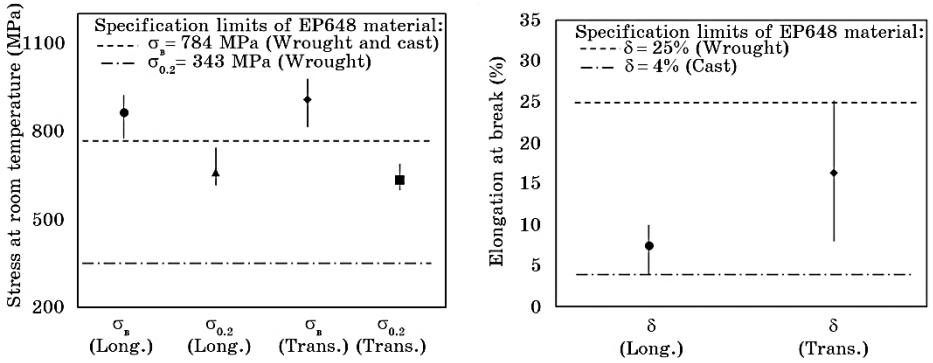

Fig. 6. Tensile-test results at room temperature for plasma-surfaced EP648 samples: (*a*) ultimate strength $\sigma_в$ and yield strength $\sigma_{0.2}$; (*b*) elongation δ.

Fig. 7. Broken samples after tensile testing at room temperature.

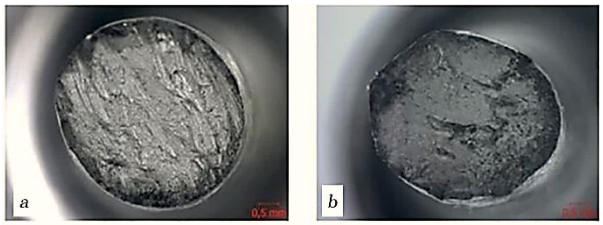

Fig. 8. Fracture surfaces of broken test bars: (*a*) longitudinal direction; (*b*) transverse direction.

specification limit of wrought material by some 70% in the longitudinal direction and 35% in the transverse direction. All samples developed a wavy surface appearance during testing with varying degrees of plastic thinning and eventually fractured with the formation of a neck.

Some typical broken samples after the tensile testing are shown in Fig. 7. No obvious defects such as porosity, oxidation, elemental segregation or oxidation were found at the fractures. The fractures appeared to have a wavy topography characterized by a number of small craters, as shown in Fig. 8. These surface features were further inspected using a binocular optical microscope and the results are presented in Fig. 9. It can be seen that the small craters were surrounded by bright reflective ridges under the microscope. These craters correspond to the individual fine grains created by plasma surfacing and the ridges were plastically deformed and fractured grain boundaries as a result of the tensile tests.

In qualifying the plasma-surfacing process in producing stator and structural components for aeroengines, further stress rupture tests were conducted by applying an axial stress of 73 MPa at an elevated temperature of 450°C. Stipulated in the part-specific EP648 material standard, the load and temperature values are representative of the actual operating conditions of the EP648 parts in the aeroengines. The

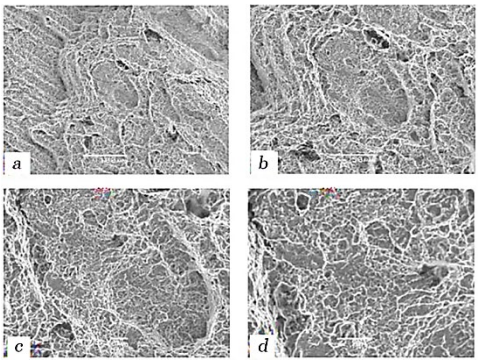

Fig. 9. Microscopic examination of fractures on broken specimens: (*a*) ×200; (*b*) ×500; (*c*) ×1000; (*d*) ×2000.

TABLE 2. Stress rupture test scheme and results of plasma-surfaced EP648 samples.

Sample direction	Q-ty	Temperature [°C]	Load [MPa]	Duration [h]	Notation
Longitudinal	3	450	73	till 200	Not broken
Transverse	3	450	73	till 200	Not broken

Part-specific requirement for wrought EP648 component: 200 hours at 73 MPa and 450 °C

stress-rupture test results are shown in Table 2, based on six randomly selected longitudinal and transverse test bars. It can be seen that both the longitudinal and transverse test bars successfully withstood 200 hours before the tests were terminated in favour of a faster turnaround in testing.

Combining the room-temperature tensile and high-temperature stress-rupture results, it is clear that the additively grown EP648 test bars using plasma-surface additive process have superior mechanical properties in comparison to castings. When compared to the wrought material, the additively grown EP648 bars demonstrated comparable strength at both room temperature and elevated ones. Only the elongation results are lower than the wrought specification limit, although most likely a lot higher than that of typical castings. In view of the negligible role of ductility in the failure modes of stator vanes and structural components in an aeroengine, obtained design approvals for the plasma-surfacing process not only as a replacement of the traditional casting process, but also for the forging process in producing EP648 components.

3.2. Component Manufacturing Trial

A manufacturing trial was conducted to produce a turbine casing using the plasma-surfacing process for a turbofan engine rated at 2500 kgf dry thrust. In the current mass production, the component is manufactured by machining a forging blank to the net shape. The plasma-surfacing trial was conducted using the same plasma equipment as for the plate samples, but with a thicker EP648 wire of 1.5 mm diameter. As shown in Fig. 10, a near-net-shape blank was produced as a circular thin-wall structure, grown on top of a steel substrate. A 10 mm-high transition layer was first deposited between the substrate and the part to create enough margins for cutting the blank off from the substrate post-deposition. Each layer of EP648 material measured approximately 3 mm in height and 15 mm in width. In total, twelve layers were deposited to complete the required geometry for the blank. Then, the blank was subject to the conventional machining processes including turning and drilling to bring it to the final geometry.

Non-destructing testing (NDT), including fluorescent penetrant inspection (FPI) and x-ray radiography, was carried out on the additively grown blank and subsequently the finished part. No unacceptable cracks, non-melting or other types of metallurgical defects were detected and the finished part was in full compliance with the part-specific quality specifications.

A cost analysis was carried out to understand the competitiveness of using the additive manufacturing route against the traditional forging-machining route when producing the same finished component. As

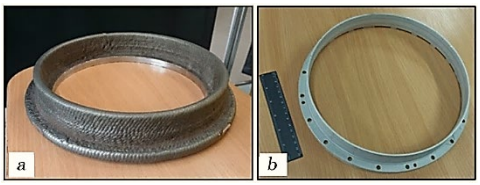

Fig. 10. Plasma surfacing trial for aero engine casing (a) additively grown blank (b) finished part after machining operations.

TABLE 3. Costs' benefit analysis result.

	Forging process	Plasma-surfacing process
Weight of finished part [kg]	2.5	2.5
Material utilization factor	0.100	0.625
Weight of blank [kg]	24.78	4.0
Unit cost of material [USD]	72 (wrought bar)	105 (extruded wire)
Total cost of material [USD]	1784	420

shown in Table 3, the analysis results clearly indicate that the additive manufacturing route has brought a significant cost benefit of nearly USD 1,400 for the turbine casing, due to a much higher material utilization factor and a relatively low superalloy wire price.

It is worth noting that the above cost estimation is solely based on material utilization. For business confidentiality reasons, tooling, hourly labour and equipment costs incurred for forging and machining the excessive blank material are not reported in this paper. However, it is apparent that the actual cost benefit brought by the plasma-surfacing process is likely to be much larger, if all cost elements are included.

Based on the technical and commercial evaluation reported above, a full part-specific process specification has been created to introduce the plasma-surfacing process into mass production for turbine and combustion casings.

4. CONCLUSIONS

The plasma-surfacing process using EP648 superalloy wire has been demonstrated to produce samples with homogeneous microstructure comparable to conventional castings. This microstructure is characterized by uniform distribution of alloying elements throughout the matrix, featuring a well-formed γ-solid solution with consistently distributed nitrides and carbonitrides. The process results in complete absence of visible fusion lines between deposited layers, while exhibiting epitaxial grain growth across layers, that indicates excellent metallurgical bonding. Notably, the resulting material displays a finer grain structure compared to cast material, which can be attributed to the accelerated cooling rates inherent to the plasma-surfacing process.

The mechanical properties evaluation at room temperature has revealed significant improvements over conventional manufacturing methods. The material demonstrates ultimate tensile strength ($\sigma_в$) that exceeds both cast and wrought material specifications, while the yield strength ($\sigma_{0.2}$) notably surpasses wrought EP648 requirements by a considerable margin. Although the elongation (δ) values exceed cast material specifications, they remain below wrought requirements, showing approximately 70% lower values in the longitudinal direction and 35% lower in the transverse direction. Detailed fracture analysis has revealed a ductile failure mode with characteristic crater formations that correspond directly to the fine grain structure of the material.

High-temperature performance testing has conclusively validated the process suitability for aerospace applications. The material has successfully passed 200-hour stress-rupture tests conducted at 450°C under 73 MPa load, with both longitudinal and transverse specimens demonstrating comparable performance levels. These results meet or

exceed the part-specific requirements for wrought EP648 components, while demonstrating the thermal stability necessary for aeroengine operating conditions. This performance validation is particularly significant for the intended application in aerospace components.

From a manufacturing efficiency and economic perspective, the plasma-surfacing process has demonstrated substantial benefits. The material utilization factor has increased dramatically from 0.100 in forging to 0.625 in plasma surfacing, resulting in a cost reduction of approximately USD 1,400 per component based on material savings alone. Even greater cost benefits are anticipated, when considering the reduced machining and tooling requirements. The process has successfully produced complex geometries such as turbine casings that meet all quality specifications, with no unacceptable defects detected through comprehensive NDT methods including FPI and x-ray radiography.

The process validation for industrial implementation has been successfully completed, qualifying the method for both cast and forged component replacement. This comprehensive validation establishes plasma surfacing as a viable alternative manufacturing method for aeroengine components, particularly in applications, where high strength and thermal stability are critical requirements. The combined results of this study conclusively validate plasma surfacing as an effective and economically advantageous manufacturing process for EP648 superalloy components in aeroengines, particularly for stator and structural parts.

AUTHORS' CONTRIBUTIONS

Mykhail Gnatenko: ideas; formulation or evolution of overarching research goals and aims; preparation, creation and/or presentation of the published work, specifically, writing the initial draft (including substantive translation); provision of study materials, reagents, materials. Hanna Laptieva: preparation, creation and/or presentation of the published work by those from the original research group, specifically critical review, commentary or revision, including pre- or post-publication stages; application of statistical, mathematical, computational, or other formal techniques to analyse or to synthesize study data. Volodymyr Yefanov: development or design of methodology; creation of models; verification, whether as a part of the activity or separate, of the overall replication/reproducibility of results/experiments and other research outputs. Oleg Kalinichenko: oversight and leadership responsibility for the research activity planning and execution, including mentorship external to the core team; management activities to annotate (produce metadata), scrub data and maintain research data (including software code, where it is necessary for interpreting the data itself) for initial use and later reuse. Radomir Osipchuk: prep-

aration, creation and/or presentation of the published work by those from the original research group, specifically, critical review, commentary or revision, including pre- or post-publication stages; preparation, creation and/or presentation of the published work, specifically, visualization/ data presentation.

REFERENCES

1. M. Gnatenko, P. Zhemanyuk, I. Petryk, S. Sakhno, S. Chigileichik, V. Naumik, A. Ovchinnikov, and M. Matkovskaya, *East.-Eur. J. Enterp. Technol.*, **1**, No. 12(97): 49 (2019).
2. V. S. Yefanov, M. O. Gnatenko, H. M. Laptieva, Y. F. Basov, K. M. Sukhyy, S. V. Kovalyov, and S. M. Popov, *Vopr. Khim. Khim. Tekhnol.*, **2024**, No. 4: 95 (2024).
3. P. Kah, H. Latifi, R. Suoranta, Jukka Martikainen, and Markku Pirinen, *Int. J. Mech. Mater. Eng.*, **9**: 15 (2014).
4. F. Martina, J. Mehnen, S. W. Williams, P. Colegrove, and F. Wang, *J. Mater. Process. Technol.*, **212**, No. 6: 1377 (2012).
5. J. P. Oliveira, B. Crispim, Z. Zeng, T. Omori, F. M. Braz Fernandes, and R. M. Miranda, *J. Mater. Process. Technol.*, **271**: 93 (2019).
6. D. Ding, Z. Pan, D. Cuiuri, and H. Li, *Int. J. Adv. Manuf. Technol.*, **81**: 465 (2015).
7. A. R. McAndrew, M. Alvarez Rosales, P. A. Colegrove, J. R. Hönnige, A. Ho, R. Fayolle, K. Eyitayo, I. Stan, P. Sukrongpang, A. Crochemore, and Z. Pinter, *Addit. Manuf.*, **21**: 340 (2018).
8. M. Gnatenko, V. Naumyk, and M. Matkovska, *Mater. Sci. Technol.*, **2019**: 68 (2019).
9. S. W. Williams, F. Martina, A. C. Addison, J. Ding, G. Pardal, and P. Colegrove, *Mater. Sci. Technol.*, **32**, No. 7: 641 (2016).
10. D. Ding, Z. Pan, S. Van Duin, H. Li, and C. Shen, *Materials*, **9**: 652 (2016).
11. F. Martina, J. Ding, S. Williams, A. Caballero, G. Pardal, and L. Quintino, *Addit. Manuf.*, **25**: 545 (2019).
12. J. P. Oliveira, D. Barbosa, F. M. Braz Fernandes, and R. M. Miranda, *Smart Mater. Struct.*, **25**: 03LT01 (2016).
13. J. P. Oliveira, F. M. Braz Fernandes, R. M. Miranda, N. Schell, and J. L. Ocaña, *Mater. Charact.*, **119**: 148 (2016).
14. F. Wang, S. Williams, and M. Rush, *Int. J. Adv. Manuf. Technol.*, **57**: 597 (2011).
15. F. Martina, J. Mehnen, S. W. Williams, P. Colegrove, and F. Wang, *J. Mater. Process. Technol.*, **212**, No. 6: 1377 (2012).
16. S. Jhavar, N. K. Jain, and C. P. Paul, *J. Mater. Process. Technol.*, **214**, No. 6: 1102 (2014).
17. S. W. Williams, F. Martina, A. C. Addison, J. Ding, G. Pardal, and P. Colegrove, *Mater. Sci. Technol.*, **32**, No. 7: 641 (2016).